Interdecadal Changes in the ENSO–Monsoon System

CHRISTOPHER TORRENCE

Advanced Study Program, National Center for Atmospheric Research, Boulder, Colorado

PETER J. WEBSTER

Program in Atmospheric and Oceanic Sciences, University of Colorado, Boulder, Colorado

(Manuscript received 29 May 1998, in final form 27 November 1998)

ABSTRACT

The El Niño–Southern Oscillation (ENSO) and Indian monsoon are shown to have undergone significant interdecadal changes in variance and coherency over the last 125 years. Wavelet analysis is applied to indexes of equatorial Pacific sea surface temperature (Niño3 SST), the Southern Oscillation index, and all-India rainfall. Time series of 2–7-yr variance indicate intervals of high ENSO–monsoon variance (1875–1920 and 1960–90) and an interval of low variance (1920–60). The ENSO–monsoon variance also contains a modulation of ENSO–monsoon amplitudes on a 12–20-yr timescale.

The annual-cycle (1 yr) variance time series of Niño3 SST and Indian rainfall is negatively correlated with the interannual ENSO signal. The 1-yr variance is larger during 1935–60, suggesting a negative correlation between annual-cycle variance and ENSO variance on interdecadal timescales.

The method of wavelet coherency is applied to the ENSO and monsoon indexes. The Niño3 SST and Indian rainfall are found to be highly coherent, especially during intervals of high variance. The Niño3 SST and Indian rainfall are approximately 180° out of phase and show a gradual increase in phase difference versus Fourier period. All of the results are shown to be robust with respect to different datasets and analysis methods.

1. Introduction

Sir Gilbert Walker knew that the Southern Oscillation (SO) and the Indian summer monsoon are intimately linked (Walker and Bliss 1937), and he hoped that knowledge of the SO would permit accurate prediction of the monsoon (Normand 1953). Since then, numerous studies have shown the influence of the Indian monsoon (hereafter simply the ''monsoon'') on tropical circulation (Normand 1953; Troup 1965; Yasunari 1990; Yasunari and Seki 1992) or, conversely, the impact of the El Niño–Southern Oscillation (ENSO) on the monsoon (Walker and Bliss 1937; Shukla and Paolino 1983; Joseph et al. 1994).

Each year during March–May, the center of tropical convection migrates from the western Pacific warm pool to the northwest, announcing the arrival of both the Southeast Asian monsoon and the Indian summer monsoon (Meehl 1987). Every few years, an El Niño (or warm) event produces a warming of the sea surface temperature (SST) in the central and eastern Pacific, accompanied by diminished easterly trade winds and an eastward shift in tropical convection. The opposite La Niña (or cold) event, which sometimes follows a warm event, produces an anomalous westward shift in warm SSTs and convection, as well as enhanced easterly trades (Rasmusson and Carpenter 1982).

The strength of the monsoon and the occurrence of warm or cold ENSO events depend on the location and magnitude of western Pacific SSTs and on tropical convection (Soman and Slingo 1997). A strong monsoon [heavy rains, low sea level pressure (SLP), strong easterlies] tends to inhibit warm events and favor cold events (Yasunari 1990). Conversely, a warm ENSO event (decreased convection and high SLP in the west Pacific, weak easterlies) tends to suppress the monsoon (Webster 1995). No cause or effect is implied (or indeed warranted) in either case.

Since the ENSO–monsoon interaction works in both directions, it is difficult to use one to forecast the other. Forecasts of either one are also complicated by the ENSO–monsoon interaction itself, which occurs ultimately on intraseasonal timescales through the Madden–Julian oscillation, the timing of monsoon onset, the modulation of monsoon active/break periods, and western Pacific westerly wind bursts (for a review see Webster et al. 1998).

Corresponding author address: Dr. Christopher Torrence, Advanced Study Program, National Center for Atmospheric Research, P.O. Box 3000, Boulder, CO 80307-3000.
E-mail: torrence@ucar.edu

Coupled ocean–atmosphere models that include both intraseasonal and interannual processes suggest that the Indian monsoon can have a large impact on ENSO and vice versa (e.g., Ju and Slingo 1995; Wainer and Webster 1996; Meehl 1997); yet this knowledge has not been effectively implemented into monsoon or ENSO forecasting systems. Some of this failure is caused by interdecadal changes in both the ENSO–monsoon system and the global ocean–atmosphere background state (Webster and Palmer 1997).

Interdecadal changes have been found in tropical rainfall (Kraus 1955; Mooley and Parthasarathy 1984), monsoonal atmospheric circulation (Fu and Fletcher 1988; Parthasarathy et al. 1991), ENSO frequency and amplitude (Gu and Philander 1995; Mak 1995; Wang and Wang 1996), and ENSO–monsoon relationships (Elliott and Angell 1988; Shukla 1995). Multidecadal and century-long changes have been found in proxy ENSO records (Cole et al. 1993; Knutson et al. 1997; Diaz and Markgraf 1992). Other studies have examined changes in mean SST (Deser and Blackmon 1995; Zhang et al. 1997), especially on the 1976–77 increase in SSTs in the Pacific Ocean (Trenberth and Hurrell 1994; Wang 1995).

Since ENSO and the monsoon have such a strong teleconnection with global climate anomalies, it is important to examine ENSO and monsoon variability. The interdecadal changes are also important in analyzing the appropriateness and robustness of theories for ENSO and the monsoon, and in determining the expected skill of ENSO–monsoon forecasts.

The purpose of this paper is to give a detailed description of the interdecadal changes in variance and coherency of the ENSO–monsoon system during the last 125 yr, along with a measure of their statistical significance. Wavelet analysis is used to isolate the timescales of ENSO–monsoon variability, and significance tests are used to assess the robustness of the results. The method of wavelet coherency is used to link ENSO and monsoon variance.

Section 2 describes the datasets used. Section 3 presents the wavelet power spectra and variance time series. Section 4 uses wavelet coherency to analyze the ENSO–monsoon relationship. Verification with other datasets is given in section 5. A summary and discussion are given in section 6. The appendix contains a description of wavelet coherency and phase.

2. Data

Three indices will be used as measures of variability in the ENSO–monsoon system: Niño3 SST, the Southern Oscillation index (SOI), and all-India rainfall. Additional datasets used for verification are described in section 5.

a. Niño3 sea surface temperature

The El Niño (or oceanic) component of ENSO is measured here by the Niño3 SST index, consisting of the area-average SST over the eastern equatorial Pacific (5°S–5°N, 90°–150°W), monthly from January 1871 to September 1998.

The 1871–1996 data is from the U.K. Meteorological Office (UKMO) Global sea-Ice and Sea Surface Temperature (GISST) 2.3-b dataset, available on a $1° \times 1°$ resolution grid (courtesy of D. Rowell and J. Arnott, UKMO). As described in Rayner et al. (1996), the GISST 2.3 b is derived from in situ ship measurements and bias-corrected satellite observations. Data-void regions (prominent for pre-1950 data) are filled using empirical orthogonal functions (EOFs). The EOFs are determined from the 1871–1994 data using anomalies from the 1960–91 climatology (Parker et al. 1995). The EOF analysis is done on a $4° \times 4°$ resolution grid and consists of a single global EOF mode (to capture any trend) and multiple EOF modes for each ocean basin (Rayner et al. 1996). A general discussion of data-quality issues for ship measurements is given in Folland et al. (1984).

The GISST data are used to provide a gridded dataset from which area-average SSTs can be calculated. This approach is thought to be more robust than using the individual ship data, as the original ship reports are not uniformly distributed over the Niño regions in either space or time.

The Niño3 SST index for January 1997–September 1998 is from the Climate Prediction Center (CPC) optimally interpolated SST (courtesy of D. Garrett, NOAA). For details of the analysis method see Reynolds and Smith (1994).

b. Southern Oscillation index (SOI)

The Southern Oscillation (or atmospheric) component of ENSO is measured by the SOI (Troup 1965), usually defined as the anomalous SLP in the eastern Pacific at Tahiti (17.6°S, 149.6°W) minus SLP in the western Pacific at Darwin, Australia (12.4°S, 130.9°E).

Monthly SLP at Tahiti and Darwin from 1876 to 1950 were provided by R. Allan (Commonwealth Scientific and Industrial Research Organisation), while 1951–September 1998 data are from CPC (courtesy of D. Garrett). The pre-1936 SLP at Tahiti are from Ropelewski and Jones (1987), while pre-1882 SLP at Darwin are from Allan et al. (1991). Data gaps and inhomogeneities were corrected using linear regression from nearby stations by Allan et al. (1996).

To measure interdecadal changes, the annual cycle is kept within each time series, and the SOI is simply defined as the monthly SLP at Tahiti minus the SLP at Darwin (note that the wavelet analysis will separate the residual annual cycle from the ENSO timescales). One possible criticism of this definition is the different SLP

variance at Darwin and Tahiti (Trenberth 1976). Most of this difference is due to the larger annual cycle at Darwin. The standard deviations (1876–1998) of SLP at Darwin and Tahiti are 2.62 and 1.68 mb, respectively; with the monthly mean annual cycle removed, the standard deviations become 1.08 and 1.06 mb, respectively. Therefore, changes in the SOI annual cycle will mostly reflect Darwin, while SOI changes on other timescales will be equally weighted between Darwin and Tahiti.

c. All-India rainfall

Indian rainfall is from the all-India rainfall index, consisting of an area-weighted average of 306 rain gauges distributed across the plains regions of India (Mooley and Parthasarathy 1984). Monthly rainfall is available from 1871 to 1994, and the mean (90.9 mm) is removed. Note that this is a monthly index and is not just the sum over the monsoon rainy season.

3. Changes in ENSO and monsoon variance

The time series of Niño3 SST, the SOI, and Indian monsoon rainfall are shown in Fig. 1. The SST and SOI have been smoothed to highlight the interannual ENSO component; however, the rest of the analysis uses the unsmoothed time series. Likewise, the Indian rainfall time series shows only the June–September total (in standard deviations from the mean), while the remainder of the paper uses the monthly time series.

The Niño3 SST and SOI are clearly 180° out of phase, as expected for the El Niño–Southern Oscillation (Rasmusson and Carpenter 1982). Both warm (El Niño) and cold (La Niña) events occur approximately every 2–7 yr, and there is considerable variability in the amplitude of ENSO events (e.g., the large 1997–98 El Niño) and in the duration of events (e.g., the prolonged 1992–95 warm anomaly). The shading on the monsoon rainfall indicates years associated with El Niño events (black bars) or La Niña events (gray bars). It is apparent that El Niño years are typically associated with deficient monsoon rainfall, while La Niña years are associated with abundant rainfall (Shukla and Paolino 1983; Yasunari and Seki 1992). The relationship is not perfect, suggesting that processes other than ENSO can have an impact on monsoon rainfall (and vice versa).

In Fig. 1, one can see evidence of three distinct time intervals: the first (1875–1920) has numerous ENSO events and large changes in monsoon rainfall, the second (1920–60) has fewer ENSO events and less monsoon variability, and the third (1960–present) again has more ENSO events and more monsoon variability. These interdecadal changes will be examined in the following sections using wavelet analysis.

a. Wavelet analysis method

To isolate the different timescales, the Niño3 SST, the SOI, and Indian rainfall are analyzed with the wavelet transform. The Morlet wavelet is used, and the transform is performed in Fourier space using the method described in Torrence and Compo (1998; hereafter TC98). Further details on wavelet analysis can be found in Foufoula-Georgiou and Kumar (1995). To reduce wraparound effects, each time series is padded with zeros. Other wavelet bases, such as the Paul and Mexican hat, were tested and gave the same qualitative results.

The Morlet wavelet consists of a complex exponential modulated by a Gaussian, $e^{i\omega_0 t/s}e^{-t^2/(2s^2)}$, where t is the time, s is the wavelet scale, and ω_0 is a nondimensional frequency. For $\omega_0 = 6$ (used here), there are approximately three oscillations within the Gaussian envelope. The wavelet scale s is almost identical to the corresponding Fourier period of the complex exponential, and the terms ''scale'' and ''period'' will be used synonymously.

The wavelet power spectrum is defined as the absolute value squared of the wavelet transform and gives a measure of the time series variance at each scale (period) and at each time. Note that the wavelet transform conserves variance, and the time series can be recovered exactly (TC98). To test the significance of peaks in the wavelet power spectrum, a background Fourier spectrum must be chosen. To test for nonstationary changes in variance, it is most appropriate to choose the global wavelet spectrum (GWS), given by the time average of the wavelet power spectrum (Kestin et al. 1998). The wavelet power spectrum is then distributed as chi-square (two degrees of freedom) about the GWS (TC98).

The global wavelet spectra are shown in Fig. 2. The GWS is equivalent to the Fourier power spectrum smoothed by the Morlet wavelet function in Fourier space (Farge 1992). Since the width of the wavelet function is constant in period (the short horizontal lines), the number of smoothed Fourier components decreases with increasing period. This implies a decrease in the degrees of freedom (DOF) with increasing period, and a corresponding increase in the width of the 95% confidence intervals (the error bars). The decrease in DOF also causes a rise in the 1% significance level with period, despite the choice of a white-noise background (TC98).

The GWS for Niño3 SST and the SOI show the annual cycle and strong 2–8-yr ''interannual'' peaks. The Indian rainfall is dominated by the annual cycle; the rest of the spectrum appears flat (i.e., white noise), except for a possible peak around 2.8 yr. The next section will analyze the variation of wavelet power about these mean spectra.

b. Wavelet power spectra

The wavelet power spectra for Niño3 SST, the SOI, and Indian rainfall are shown in Fig. 3. The wavelet power is normalized by dividing each month by the GWS (Fig. 2), and thus it measures the deviations from the mean spectrum. The thick black contours indicate

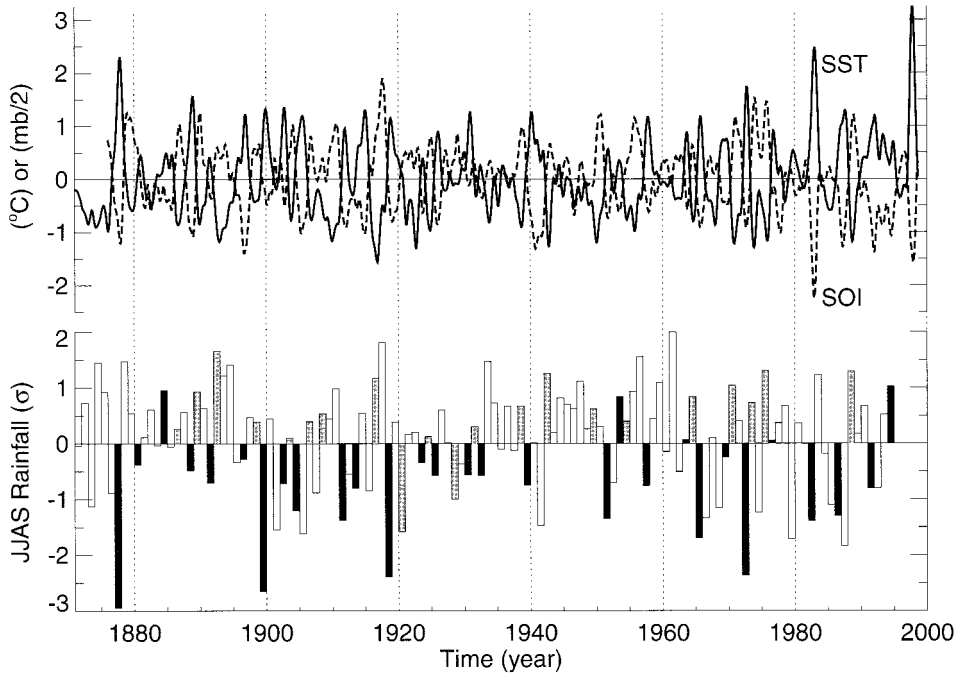

FIG. 1. Time series of Niño3 SST (solid curve, °C), the SOI (dashed curve, mb/2), and the Jun–Sep (JJAS) total monsoon rainfall (bars; mean = 853 mm, standard deviation σ = 84.2 mm). For presentation purposes, the monthly mean annual cycles have been removed, and the SST and SOI have been smoothed by an 11-month Lanczos filter (Trenberth 1984). For the monsoon rainfall, black bars indicate El Niño year (0)s and gray bars indicate La Niña year (0)s, as defined by Kiladis and Diaz (1989).

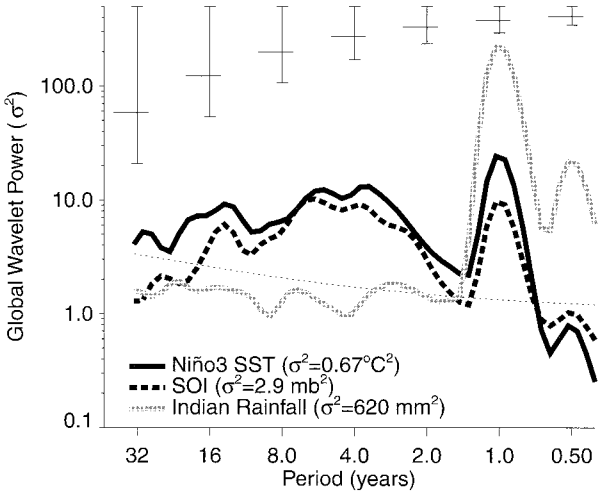

FIG. 2. The global wavelet power spectra for Niño3 SST (solid line), the SOI (dashed line) and the all-India rainfall (gray line), as a function of Fourier period. The dotted line is the 1% significance level for all three, assuming a white noise process. Before computing variances (σ^2) and significance levels, the time series were prewhitened by removing the monthly mean annual cycle; the annual cycle was then reinstated. The vertical error bars represent the 95% confidence interval (on a logarithmic scale) for each of the curves (for clarity the bars are only plotted for every power of 2). The horizontal lines across each error bar indicate both the baseline of the error bar, and the width of the wavelet function in Fourier space.

regions that are significant (at the 10% level) above the GWS.

For Niño3 SST and the SOI (Figs. 3a,b), the power is broadly distributed, with peaks in the 2–8-yr ENSO band. The 10% significance regions indicate that 1875–1920 and 1960–90 contain intervals of higher ENSO variance, while 1920–60 is a time of lower ENSO variance. Similar variance changes are found in east Pacific SST and Darwin SLP (Wang and Wang 1996), and in tropical zonal winds (Gu and Philander 1995). Here, the use of significance tests allows one to verify that the interdecadal variance changes in ENSO are statistically significant (Torrence and Webster 1998).

The wavelet spectrum for all-India rainfall (Fig. 3c) is more uniformly distributed about all periods, as can also be seen in the GWS. The 1–8-yr band shows interdecadal changes similar to Niño3 SST and the SOI, with a distinct time of low variability from 1920 to 1950. Normand (1953) also noted a decrease in the severity of drought/flood events after 1920.

The tropical biennial oscillation (TBO), or 2-yr band, is not especially pronounced, except perhaps in the rainfall. Since the TBO is thought to occur irregularly (Meehl 1997), the Morlet wavelet (which has three oscillations) is perhaps not the best wavelet function to use. Nevertheless the 2-yr variance shows the same decrease from 1920 to 1960 as the 2–8-yr band. There is also power in the 8–20-yr band during the last 50 yr,

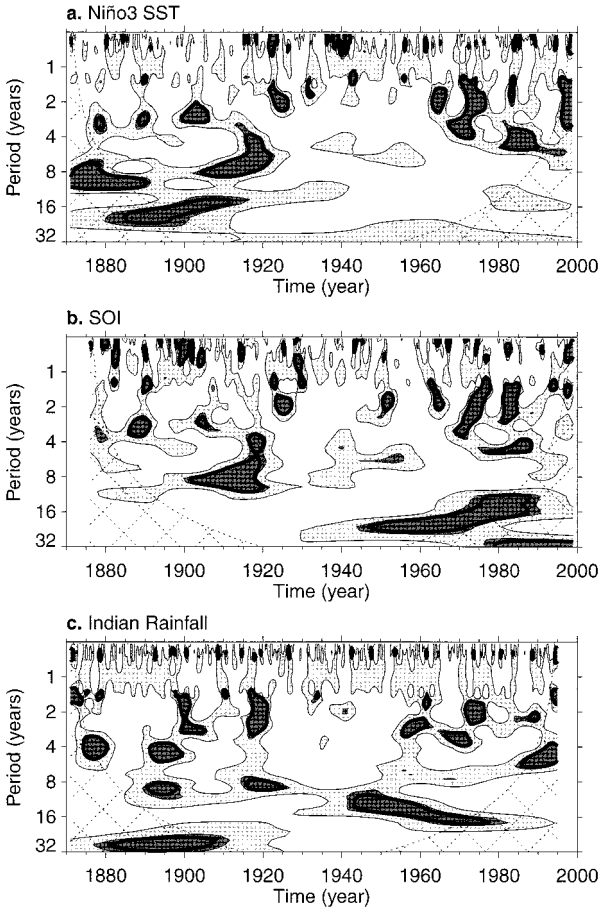

FIG. 3. (a) Wavelet power spectrum (using the Morlet wavelet) of the Niño SST. The wavelet power at each period is normalized by the global wavelet spectrum (GWS; Fig. 2). The shaded contour levels are at 1 and 2, i.e., ''equal to the GWS'' and ''twice the GWS,'' respectively. Cross-hatched regions indicate the ''cone-of-influence,'' where zero padding has reduced the variance. The thick black contour is the 10% significance level above the GWS. (b) Same as (a) but for the SOI. (c) Same as (a) but for all-India rainfall.

which agrees with the results of Mooley and Parthasarathy (1984).

The wavelet power spectra for Niño3 SST, the SOI, and all-India rainfall indicate that there is significant (at 10%) nonstationary in variance in the 2–8-yr ENSO band. The variance changes also appear to agree on some of the finer-detail features, especially in the 2–4-yr band. These features are more easily seen in the variance time series.

c. Time series of 2–7-yr variance

To clarify the interdecadal changes in interannual variance, Fig. 4 shows the 2–7-yr wavelet variance times series (thick black curves with shading). Each horizontal slice through Fig. 3 represents a time series of wavelet variance at a particular scale (relative to the GWS). The wavelet power spectra are converted to energy densities by first multiplying by the GWS (to remove the normalization) and then dividing each time series by its corresponding wavelet scale. The 2–7-yr time series of energy density is then summed (TC98). Due to the scale width of the Morlet wavelet, the results are similar for scale averages using 2–5 yr or 3–7 yr. The above method is also equivalent to using a Fourier bandpass filter: the variance is conserved, and the mean amplitude of the variance time series is equal to the total variance within the bandpass filter (TC98).

The 2–7-yr variance time series of Niño3 SST, SOI, and all-India rainfall (Fig. 4) show large changes over the last 125 yr, with high variance from 1875 to 1920, lower variance from 1920 to 1960, and then high variance from 1960 to 1990. The three variance time series are highly correlated with each other, with the Spearman rank correlations given in Table 1 (the rank correlation is used because the time series are not Gaussian distributed). The significance levels are determined from Student's t-distribution, with the degrees of freedom estimated using a decorrelation time of 5.2 yr, determined from the *e*-folding time of the 2–7-yr scale-averaged wavelet.

In addition to the 1875–1920/1920–60/1960–90 interdecadal change in variance, there is also a 12–20-yr ''oscillation'' in variance, which is especially prominent in 1875–1920 and 1960–90 (Torrence and Webster 1998). The thin curves in Fig. 4 are the square of the 2–7-yr bandpass-filtered time series. The black shading indicates where the filtered time series was originally positive in Niño3 SST, or negative in the SOI and Indian rainfall.

For Niño3 SST and the SOI the 12–20-yr variance oscillation corresponds to a 12–20-yr amplitude modulation of ENSO events. The ENSO system seems to go through an irregular cycle of increasing amplitude of ENSO events followed by decreasing amplitude. The 12–20-yr cycle is clearly apparent in 1875–1920 and 1960–90, but less apparent for 1920–60. This modulation was also found in central Pacific SST from 1949 to 1992 by Mak (1995). For all-India rainfall the 12–20-yr modulation is not as well defined, yet there are still intervals of correspondence between ENSO variance and all-India rainfall variance (e.g., 1871–85, 1895–1925, 1960–90). The intervals of high ENSO–monsoon correspondence are more apparent in the wavelet coherency (section 4).

d. Time series of annual-cycle variance

The annual-cycle variance of Niño3 SST (relative to the GWS) is given by a slice at 1-yr period through Fig. 3a. The time series of 1-yr variance for Niño3 SST and Indian rainfall (not shown) are rank correlated at 0.48 (1% significant). When the amplitude of the SST annual cycle in the eastern Pacific is large, the amplitude of the Indian rainfall annual cycle also tends to be large. The other rank correlations are given in Table 1.

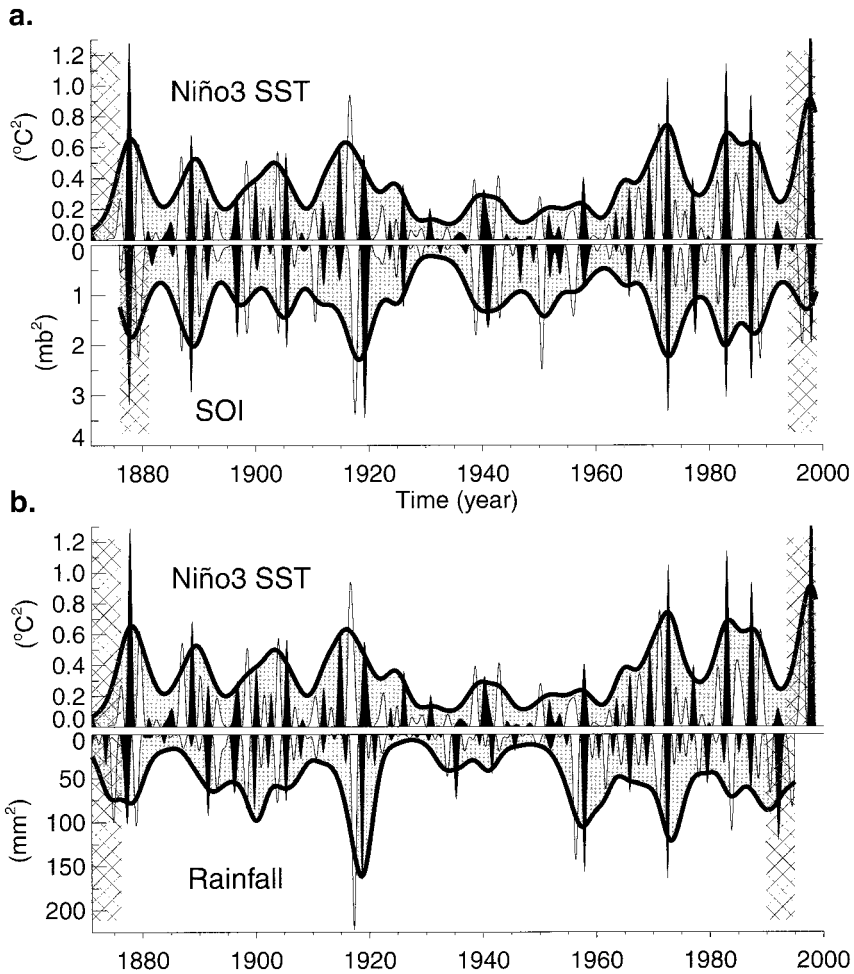

FIG. 4. (a) The upper half is the 2–7-yr variance time series for Niño3 SST (thick black curve with gray shading). The thin curve is $\frac{1}{2}$(Niño3 SST)^2, where the Niño3 SST is bandpass filtered from 2- to 7-yr using a wavelet filter. The black shading indicates positive peaks in the filtered time series (i.e., before squaring), while the white are negative peaks. The lower half is the same but for the SOI (with variance increasing downward); the black bars now indicate *negative* peaks in the filtered SOI. (b) The upper half is the same as in (a), while the lower half is for the all-India rainfall; the black bars indicate negative peaks in the filtered rainfall. In all plots the hatched bands show where zero padding has reduced the variance.

TABLE 1. Spearman rank correlation (×100) between wavelet-derived time series. Niño3′ is the 2–7-yr bandpass-filtered SST. Italics indicates significant at the 5% level, while bold are significant at the 1% level. The degrees of freedom (DOF) are estimated from the wavelet *e*-folding time (for each correlation the smaller of the two DOF is used).

	2–7-yr variance			1-yr variance		
	Niño3	SOI	Rain	Niño3	Rain	DOF
Niño3 (2–7)	—					22
SOI (2–7)	**76**	—				21
Rain (2–7)	**55**	32	—			22
Niño3 (1-yr)	−25	−04	−11	—		93
Rain (1-yr)	*−43*	−25	−07	**48**	—	91
Niño3′	*	*	*	*−29*	−23	45

* Zero by construction.

For Niño3 SST, the 1-yr variance is negatively correlated with the 2–7-yr bandpass filter ($r = -0.29$, 5% significant). This agrees with Gu and Philander (1995), who found that during El Niño events the SST annual cycle has a smaller amplitude, while during La Niña the SST annual cycle is larger. This is due to the phase locking of ENSO events to the annual cycle. In the eastern equatorial Pacific, ENSO events tend to peak in December–February, when the sea surface temperature is normally low. A warm event produces above-normal SSTs during the cooler phase of the annual cycle (weakening the annual cycle), while a cold event produces below-normal SSTs (strengthening the annual cycle).

Gu and Philander (1995) could find no relationship between interdecadal changes in ENSO and annual-cycle variance. Figure 3a suggests, however, that there is

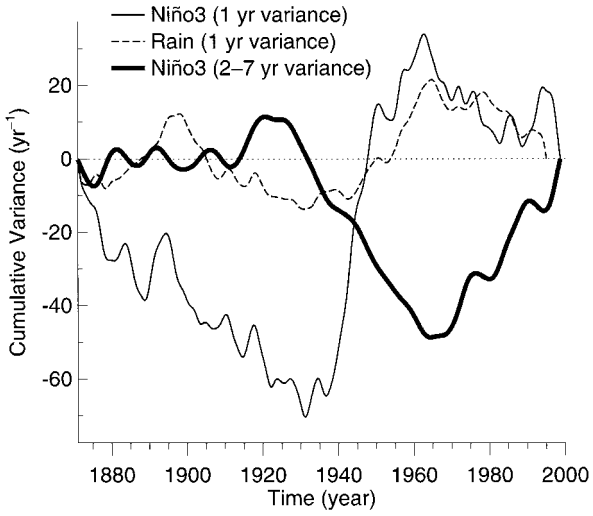

FIG. 5. Cumulative variance curves for the 1-yr Niño3 SST variance (thin solid curve), the 1-yr Indian rainfall variance (thin dashed curve), and the 2–7-yr Niño3 SST variance (thick curve), using the variance time series from Fig. 3. Before calculating, each time series was normalized by dividing by the mean, subtracting 1.0, and dividing by the average wavelet scale (either 1.0 or 3.67 yr).

higher 1-yr power from 1935 to 1960, at the same time as there is lower 2–7-yr power. Cole et al. (1993), using proxy rainfall at Tarawa (1°N, 172°E), also found increased 1-yr power from 1930 to 1955 and decreased 2–5-yr power from 1925 to 1955. Note in Fig. 3b, however, that the higher 1-yr power is not seen in the SOI.

To clarify the relationship between annual-cycle and ENSO variance, Fig. 5 shows the cumulative curves for the 1- and 2–7-yr variance time series. The cumulative value is defined as the sum of the time series from an initial time up to a certain time. Before calculating the cumulative variance, the time series was normalized by the mean variance. Upward trends in the cumulative variance indicate intervals of above-normal variance, while upward concavity indicates intervals of increasing variance (Kraus 1955).

The cumulative variance indicates that during intervals of high ENSO variance (1875–1920 and 1960–90) the annual-cycle variance is lower than average for both Niño3 SST and all-India rainfall. Conversely, during the 1920–60 interval of low ENSO variance there is higher than average annual-cycle variance. This inverse relationship also appears at the 12–20-yr timescale, especially during 1875–1910. The apparent phase shift between the 1- and 2–7-yr cumulative Niño3 variance on short timescales (prominent from 1875 to 1910) is due to the more rapid variation of the 1-yr variance, which causes changes in cumulative variance to appear earlier.

To test for significance, a Monte Carlo of 10 000 white noise time series was used with the above analysis method. None of the peaks in Fig. 5 is significant (10% level), which could suggest that the ENSO and monsoon time series are stationary in the 1- and 2–7-yr bands. Nevertheless, it should be noted that the cumulative variance method is very sensitive to the white noise assumption, which is not necessarily appropriate for the annual cycle or ENSO timescales.

4. Wavelet coherency and phase

The Fourier squared coherency is used to identify frequency bands within which two time series are covarying. Here, the wavelet squared coherency is used to identify both frequency bands and time intervals within which ENSO and the Indian monsoon are covarying. The equations for wavelet coherency and phase are given in the appendix. Henceforth, the term ''coherency'' refers to the wavelet squared coherency.

The wavelet coherency between Niño3 SST and all-India rainfall is shown in Fig. 6. The 5% significance level was determined from a Monte Carlo simulation of 10 000 sets of two white noise time series with the same length as Niño3 SST and rainfall. The SST and rainfall show significant coherency in the 1- and 2–8-yr bands, with low coherency outside of these periods. The interdecadal change in ENSO–monsoon variance appears as an interval of low coherency from 1920 to 1960, especially in the 2–4-yr band. For 1920–60, Trenberth and Shea (1987) found weakened covariance for Darwin versus Pambam, India, while Allan et al. (1996) found weakened spatial correlation patterns between ENSO indexes and SST and SLP. From 1950 to 1990 there is a shift in the period of maximum coherency from around 7 yr down to around 2 yr. This shift also appears in the coherency of Niño3 SST and the SOI (not shown).

The usefulness of the wavelet coherency is especially apparent for intervals where both wavelet power spectra (Figs. 3a,c) show minimal power, yet there is still high coherency. For example, in 1935–45 there is a high coherency peak at the 2-yr period, which corresponds to the 1939–42 sequence of El Niño/La Niña events coupled to weak/strong monsoons (see Fig. 1). The peak in 1945–55 at 5 yr corresponds to a cycle of cold/warm/cold Niño SST (4 yr each) coupled to a cycle of strong (9 yr)/weak (2 yr)/strong (4 yr) monsoons. These results suggest that even during times of low ENSO–monsoon relationship, the two phenomena can still show occasional strong interactions.

The wavelet coherency between Niño3 SST and the SOI (not shown) is greater than 0.8 for most times in the 2–8-yr band, and it exceeds 0.95 during the high ENSO variance intervals from 1875 to 1910 and 1960 to 1990. In Niño3 SST–SOI there is low coherency outside of 2–8 yr, suggesting that independent processes (e.g., noise) operate at the smallest and largest scales.

The vectors in Fig. 6 indicate the phase difference between Niño3 SST and all-India rainfall at each time and period (see key). For clarity, only one vector is plotted every 2 yr, and every other vector is plotted in the period direction (because of the timescale averaging no information is lost).

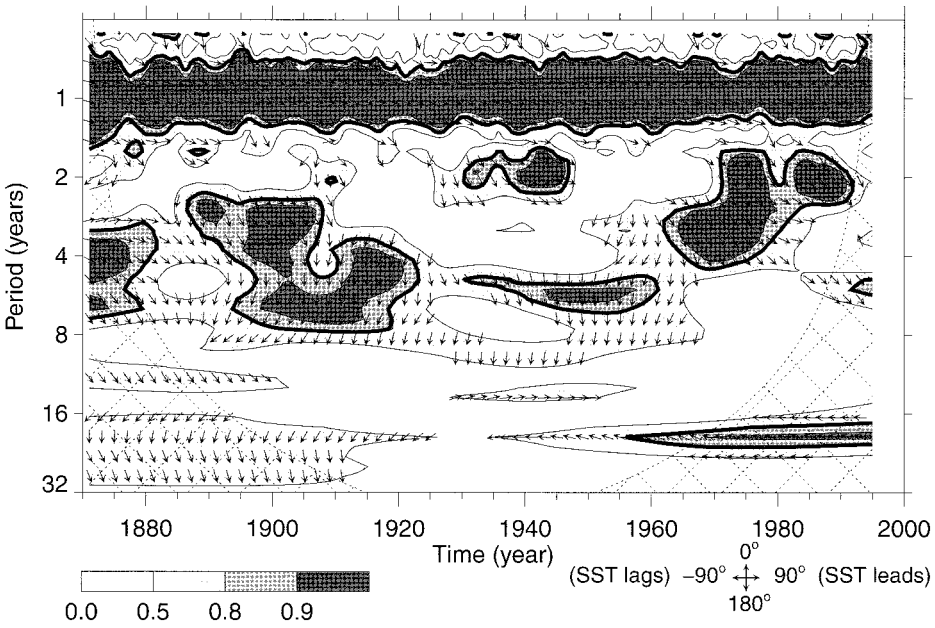

FIG. 6. The wavelet coherency and phase between Niño3 SST and all-India rainfall. Contours are for wavelet squared coherencies of 0.5, 0.8, and 0.9. The thick black contour is the 5% significance level from a Monte Carlo simulation of wavelet coherency between 10 000 sets (two each) of white noise time series. The vectors indicate the phase difference between Niño3 SST and rainfall (key in the lower right corner). For clarity, vectors are only plotted for coherency >0.5, only one vector is plotted every 2 yr in time, and every other vector is plotted in period. Cross-hatched regions indicate the cone of influence.

In the annual-cycle (1 yr) band the Niño3 SST and rainfall are about 120° out of phase. The peak SST in Niño3 occurs around April, while the peak Indian rainfall occurs around August, corresponding to a 4-month (120°) phase difference. This phase difference appears constant over the 1871–1994 record.

In the 2–8-yr band the Niño3 SST and rainfall are approximately 180° out of phase, indicating that abundant rainfall years tend to be associated with cold events, while drought years tend to be associated with warm events. For periods outside 2–8 yr the phase difference is more random.

The phase difference (rainfall lagging SST) increases from about 120° near the 2-yr band to about 180° near the 8-yr band (see especially 1875–1910 and 1930–50). This phase increase is related to the lag between the Indian monsoon season and the typical boreal winter peak of ENSO events. Figure 7a shows the regression of November–January (NDJ) Niño3 SST onto individual months of Niño3 SST and all-India rainfall for one year before, during, and after the NDJ season. During an El Niño (year 0) the Indian monsoon tends to be weaker, yet the weak monsoon actually occurs approximately 4 months before the peak Niño3 SST (depending on the El Niño; see Webster et al. 1998). Similarly, Fig. 7b shows the regression of June–September all-India rainfall onto Niño3 SST and all-India rainfall, and it indicates that a strong monsoon (year 0) is associated with cold Niño3 SST, which peaks about four months after the monsoon. Both scenarios produce a phase shift of 8 months between Niño3 SST and all-India rainfall. On a biennial timescale this implies that Niño3 SST leads rainfall by 120° (or, equivalently, Niño3 SST lags by 240°). On interannual timescales the 4-month seasonal lag becomes irrelevant and the phase difference approaches 180° out of phase.

Figure 7 also contains a distinct biennial cycle, especially for rainfall. Weak monsoons tend to be followed the next year by decreased June rainfall (possibly indicating delayed onset) yet more rainfall overall. Strong monsoons are followed the next year by increased June rainfall (possibly earlier onset) with less rainfall overall.

5. Verification with other datasets

There are numerous data-quality issues (especially pre-1950) for the GISST dataset, which include changes in measurement methods and inadequate spatial and temporal coverage. In addition, the large-scale patterns of SST and SLP associated with ENSO are continually changing, making it difficult to regard a single time series as representative of long-term ENSO activity (Trenberth 1976; Trenberth 1997).

To check the robustness of the interdecadal changes in ENSO and Indian rainfall, all of the above wavelet analyses were repeated using the following datasets and indexes:

1) Using the GISST data, all four Niño regions: Niño1+2 (10°S–0°N, 80°–90°W), Niño3 (5°S–5°N,

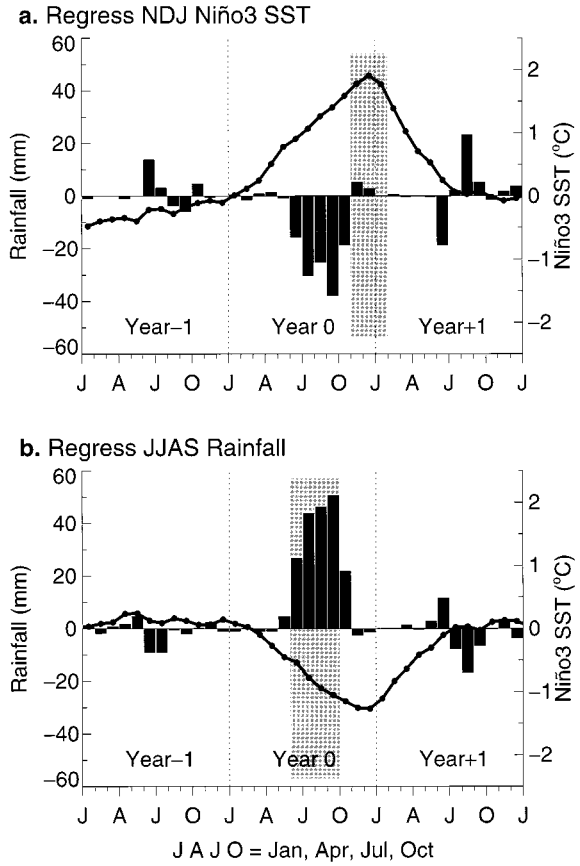

FIG. 7. (a) The linear regression of average Nov–Jan (NDJ; shaded) Niño3 SST (1872–1993; 122 points) onto Niño3 SST (black curve) and Indian rainfall (bars) for each month preceeding (year − 1), during (year 0), and following (year + 1) the NDJ season. To simulate realistic amplitudes, a regression of +2 standard deviations was used. The monthly mean annual cycle was removed from both time series. (b) Same as (a), but for the linear regression of total Jun–Sep (JJAS; shaded) all-India rainfall onto Niño3 SST and all-India rainfall.

90°–150°W), Niño3.4 (5°S–5°N, 120°–170°W), and Niño4 (5°S–5°N, 160°E–150°W);

2) The Niño3 SST index, from January 1950 to September 1998, using data from the Climate Prediction Center optimally interpolated SST [courtesy of D. Garrett, NOAA; see Reynolds and Smith (1994)]; and
3) Wright's (1989) indexes of central Pacific SST (''*S*''; monthly 1881–1986), equatorial Pacific rainfall (''*R*''; monthly 1894–1982), and Darwin minus Tahiti pressure (''*DT*''; seasonal 1870–1984); these indexes are corrected for inhomogeneities according to Wright (1989).

The results using these datasets are consistent with all of the wavelet results of the previous sections. The wavelet power spectra (e.g., Fig. 3) for all time series show nearly identical patterns. The 2–7-yr variance time series (e.g., Fig. 4) contain both the interdecadal changes and the 12–20-yr modulation. The rank correlations between the 2–7-yr variance time series are highly significant and are given in Table 2.

The long-term changes in variance are also robust to other analysis techniques. The 1920–60 variance minimum appears when using either a running 15-yr variance, or using a sliding 15-yr window Fourier power spectrum (not shown).

The interdecadal changes in ENSO–monsoon variance appear to be independent of the datasets used or the analysis method.

6. Summary and discussion

The ENSO and Indian monsoon have undergone considerable interdecadal changes in variance and coherency over the last 125 yr. The following results were shown.

- Wavelet power spectra (Fig. 3) and variance time series (Fig. 4) show interdecadal changes in 2–7-yr variance, and indicate intervals of high variance (1875–1920 and 1960–90) and an interval of low variance (1920–60).
- The 2–7-yr variance time series contain a 12–20-yr oscillation (Fig. 4), consisting of a 12–20-yr modulation of ENSO and monsoon amplitude.
- The annual-cycle variance is negatively correlated with the interannual ENSO signal (Table 1), agreeing with Gu and Philander (1995).

TABLE 2. Spearman rank correlation (×100) between 2–7-yr variance time series. Italics indicates significant at the 5% level, while bold are significant at the 1% level. The significance levels use a 5.2-yr *e*-folding time for the degrees of freedom.

	GISST				CPC	Wright		
	Niño1+2 1871–1998	Niño3 1871–1998	Niño3.4 1871–1998	Niño4 1871–1998	Niño3 1950–98	*S* 1881–1986	*R* 1894–1982	*dt* 1870–1984
GISST Niño3	**80**	—						
GISST Niño3.4	**74**	**97**	—					
GISST Niño4	**72**	**87**	**93**	—				
CPC Niño3	**87**	**96**	**91**	*71*	—			
Wright *S*	**73**	**88**	**88**	**85**	*85*	—		
Wright *R*	*58*	**83**	**82**	**77**	82	**85**	—	
Wright *dt*	**63**	**67**	**61**	*47*	*83*	**64**	**79**	—
SOI	**58**	**76**	**74**	**64**	**87**	**70**	**85**	**83**

- The annual-cycle variance appears to be negatively correlated with ENSO variance on interdecadal timescales (Fig. 5), with higher annual-cycle variance (from 1935 to 1960) during the interval of low ENSO variance.
- The wavelet coherency between Niño3 SST and all-India rainfall is very high (Fig. 6), especially in the 2–8-yr band during intervals of high variance (1875–1920 and 1960–90).

All of the results are robust with respect to different datasets and indices (Table 2), and different analysis methods (running variance and Fourier spectra).

Currently, there is no explanation for either the long-term or 12–20-yr changes in ENSO–monsoon variance and coherency, although the results suggest three possible explanations.

1) The changes in variance are part of the *internal* variability of the tropical climate system. Using simple dynamical models, Lorenz (1991) found extended intervals, ''longer than any built-in timescale,'' of one type of dynamical behavior, followed by long intervals of different behavior. In this context, 1875–1920 and 1960–90 exhibit one behavior, while 1920–60 exhibits a different behavior. Large changes in ENSO variance have been found in a low-resolution coupled ocean–atmosphere GCM, without any changes in extratropical or external forcing (Knutson et al. 1997). The Cane–Zebiak model, commonly used for ENSO forecasts, also contains interdecadal changes in ENSO amplitude and frequency, again with no changes in forcing (Zebiak and Cane 1991).
2) The changes in variance could be linked to *external* changes in the mean background climate or to extratropical changes in variance. Field correlations of 2–7-yr SST variance time series (not shown) indicate possible links on interdecadal timescales to the North Pacific, although the results are very preliminary. Connections exist between SSTs in the central equatorial Pacific and the North Pacific (Deser and Blackmon 1995; Mak 1995), and possibly between the ENSO–monsoon system and the North Atlantic oscillation (Yasunari and Seki 1992). Other studies suggest that changes in Pacific Ocean climate can influence ENSO–monsoon variability (Parthasarathy et al. 1991; Trenberth and Hurrell 1994; Wang 1995; Wang and Ropelewski 1995).
3) A combination of the previous explanations, where internal variability is modulated in part by external changes. Using the Cane–Zebiak model coupled to a simple statistical atmosphere, Kirtman and Schopf (1998) suggest that interdecadal changes in ENSO are caused by internal variability that manifests itself as changes in the mean tropical climate. Conversely, Gu and Philander (1997) propose an interdecadal oscillation of subsurface temperature anomalies between the extratropics and Tropics, causing changes in tropical SSTs and a modulation of ENSO variability.

Given the limited data record and the difficulty of separating the different timescales, it is uncertain which (if any) of the above scenarios is correct.

The increase in annual-cycle variance during times of decreased 2–7-yr variance suggest a possible ''transfer'' of energy between the the annual cycle and ENSO, occurring on interdecadal timescales. The annual cycle during 1935–60 may have been more efficient at redistributing heat throughout the Tropics, thereby reducing the amplitude and frequency of ENSO events. These changes in variance may also be related to a shift in monsoonal circulation from ''meridional'' to ''zonal'' around 1940 (Fu and Fletcher 1988; Parthasarathy et al. 1991), although the relationship and timing are unclear.

The interdecadal changes in wavelet coherency between Niño3 SST and all-India rainfall closely parallel the interdecadal variance changes, suggesting that intervals of high variance are associated with clear ENSO–monsoon relationships, and intervals of low variance show little ENSO–monsoon relationship. The variance–coherency relationship could help in assessing model predictive skill: times of high variance would presumably have higher predictive skill for both the monsoon and ENSO, due to an increase in the usefulness of the ENSO–monsoon connection. Indeed, Walker's monsoon ''foreshadowing'' was successful up until the early 1920s when the SOI–monsoon connection became weaker (Normand 1953). During 1920–60 the low coherency perhaps indicated that other processes (such as Eurasian snow cover) needed to be considered for successful monsoon forecasts. It is interesting to note that from 1921 to 1950 Australian rainfall shows both low persistence and a weakened correlation with the SOI (Simmonds and Hope 1997), suggesting that changes in ENSO variance may also affect the predictability of the Australian monsoon.

During the last 30 years it has become possible to successfully forecast ENSO events up to a year in advance (Webster and Palmer 1997). The strong ENSO–monsoon connection suggests that there is some predictability for the coupled ENSO–monsoon system (Ju and Slingo 1995). Nevertheless, Shukla (1995) notes that ''the relationship between El Niño and the Indian monsoon . . . does not hold during the most recent decade.'' As an example, 1994 was an El Niño year, yet the Indian monsoon was unusually strong (Soman and Slingo 1997). Similarly, the 1997 El Niño started unusually early and became very intense, yet the monsoon was close to normal (Webster and Palmer 1997). It is possible that the tropical climate system is returning to a period similar to 1920–60, with low ENSO–monsoon variability and reduced predictability.

Further work is needed on the cause of interdecadal variance changes in the ENSO–monsoon system, on the relationship between annual-cycle and ENSO variance,

and on the link between variance changes in the Tropics and extratropics.

Acknowledgments. Thanks to Drs. G. Compo, C. Deser, R. Madden, C. Penland, K. Trenberth, and W. Welch. The GISST dataset was kindly provided by D. Rowell, J. Arnott, and the U.K. Hadley Centre Meteorological Office. The Darwin and Tahiti SLP were kindly provided by R. Allan (CSIRO) and D. Garrett (NOAA). This work was funded in part by the NOAA Office of Global Programs Grant NA56GP0230 and National Science Foundation Grants ATM9526030 and ATM9525860. The National Center for Atmospheric Research is sponsored by the National Science Foundation.

APPENDIX

Wavelet Coherency and Phase

Traditionally, Fourier coherency has been used to identify frequency bands where two time series are related. One would like to develop a wavelet coherency, which could identify both frequency bands and time intervals when the time series were related (Liu 1994). In Fourier analysis, it is necessary to smooth the cross spectrum before calculating coherency (which is otherwise identically equal to 1). In previous studies, it was unclear how to smooth the cross-wavelet spectrum to define an appropriate wavelet coherency (Liu 1994). Here, the wavelet coherency is defined using smoothing in both time and scale, with the amount of smoothing dependent on both the choice of wavelet and the scale.

Given two time series X and Y, with wavelet transforms $W_n^X(s)$ and $W_n^Y(s)$, where n is the time index and s is the scale, the cross-wavelet spectrum is defined as

$$W_n^{XY}(s) = W_n^X(s) W_n^{Y*}(s), \tag{A1}$$

where (*) indicates complex conjugate. The cross-wavelet spectrum accurately decomposes the Fourier co- and quadrature-spectra into timescale space.

The wavelet squared coherency is defined as the absolute value squared of the smoothed cross-wavelet spectrum, normalized by the smoothed wavelet power spectra,

$$R_n^2(s) = \frac{|\langle s^{-1} W_n^{XY}(s)\rangle|^2}{\langle s^{-1}|W_n^X(s)|^2\rangle \langle s^{-1}|W_n^Y(s)|^2\rangle}, \tag{A2}$$

where $\langle \cdot \rangle$ indicates smoothing in both time and scale. Note that in the numerator, both the real and imaginary parts of the cross-wavelet spectrum are smoothed separately before taking the absolute value, while in the denominator it is the wavelet power spectra (after squaring) that are smoothed. The factor s^{-1} is used to convert to an energy density. Using these definitions, $0 \le R_n^2(s) \le 1$. Finally, it is noted that because the wavelet transform conserves variance (TC98), the wavelet coherency is an accurate representation of the (normalized) covariance between the two time series.

The wavelet-coherency phase difference is given by

$$\phi_n(s) = \tan^{-1}\left(\frac{\Im\{\langle s^{-1} W_n^{XY}(s)\rangle\}}{\Re\{\langle s^{-1} W_n^{XY}(s)\rangle\}}\right). \tag{A3}$$

The smoothed real ($\Re$) and imaginary ($\Im$) parts should have already been calculated in (A2). Both $R_n^2(s)$ and $\phi_n(s)$ are functions of the time index n and the scale s.

The smoothing in (A2) and (A3) is done using a weighted running average (or convolution) in both the time and scale directions. It should be noted that just as the Fourier coherency depends on an arbitrary smoothing function, so also does the wavelet coherency. Nevertheless, the width of the Morlet wavelet function in both time and Fourier space provides a ''natural'' width of the smoothing function. The time smoothing uses a filter given by the absolute value of the wavelet function at each scale, normalized to have a total weight of unity. For the Morlet wavelet this is just a Gaussian, $e^{-t^2/(2s^2)}$. The scale smoothing is done using a boxcar filter of width δj_0, the scale-decorrelation length. For the Morlet wavelet, $\delta j_0 = 0.60$ (TC98). Using different filter widths and shapes produces either smoother (and larger) coherency or noisier (smaller) coherency yet still gives the same qualitative results. The above filters are the best ''compromise,'' as they provide the minimal amount of smoothing necessary to include two independent points in both the time and scale dimensions.

REFERENCES

Allan, R. J., N. Nicholls, P. D. Jones, and I. J. Butterworth, 1991: A further extension of the Tahiti–Darwin SOI, early ENSO events, and Darwin pressure. *J. Climate,* **4,** 743–749.

——, J. A. Lindesay, and D. E. Parker, 1996: *El Niño Southern Oscillation and Climatic Variability.* CSIRO, 408 pp.

Cole, J. E., R. G. Fairbanks, and G. T. Shen, 1993: Recent variability in the Southern Oscillation: Isotopic results from a Tarawa atoll coral. *Science,* **260,** 1790–1793.

Deser, C., and M. L. Blackmon, 1995: On the relationship between tropical and North Pacific sea surface temperature variations. *J. Climate,* **8,** 1677–1680.

Diaz, H. F., and V. Markgraf, Eds., 1992: *El Niño: Historical and Paleoclimatic Aspects of the Southern Oscillation.* Cambridge University Press, 476 pp.

Elliott, W. P., and J. K. Angell, 1988: Evidence for changes in Southern Oscillation relationships during the last 100 years. *J. Climate,* **1,** 729–737.

Farge, M., 1992: Wavelet transforms and their applications to turbulence. *Annu. Rev. Fluid Mech.,* **24,** 395–457.

Folland, C. K., D. E. Parker, and F. E. Kates, 1984: Worldwide marine temperature fluctuations 1856–1981. *Nature,* **310,** 670–673.

Foufoula-Georgiou, E., and P. Kumar, Eds., 1995: *Wavelets in Geophysics.* Academic Press, 373 pp.

Fu, C.-B., and J. Fletcher, 1988: Large signals of climatic variation over the ocean in the Asian monsoon region. *Adv. Atmos. Sci.,* **5,** 389–404.

Gu, D., and S. G. H. Philander, 1995: Secular changes of annual and interannual variability in the Tropics during the past century. *J. Climate,* **8,** 864–876.

——, and ——, 1997: Interdecadal climate fluctuations that depend on exchanges between the Tropics and extratropics. *Science,* **275,** 805–807.

Joseph, P. V., J. K. Eischeid, and R. J. Pyle, 1994: Interannual var-

iability of the onset of the Indian summmer monsoon and its association with atmospheric features, El Niño, and sea surface temperature anomalies. *J. Climate,* **7,** 81–105.

Ju, J., and J. Slingo, 1995: The Asian summer monsoon and ENSO. *Quart. J. Roy. Meteor. Soc.,* **121,** 1133–1168.

Kestin, T. A., D. J. Karoly, J.-I. Yano, and N. A. Rayner, 1998: Time–frequency variability of ENSO and stochastic simulations. *J. Climate,* **11,** 2258–2272.

Kiladis, G. N., and H. F. Diaz, 1989: Global climatic anomalies associated with extremes in the Southern Oscillation. *J. Climate,* **2,** 1069–1090.

Kirtman, B. P., and P. S. Schopf, 1998: Decadal variability in ENSO predictability and prediction. *J. Climate,* **11,** 2804–2822.

Knutson, T. R., S. Manabe, and D. Gu, 1997: Simulated ENSO in a global coupled ocean–atmosphere model: Multidecadal amplitude modulation and CO_2 sensitivity. *J. Climate,* **10,** 138–161.

Kraus, E. B., 1955: Secular changes of tropical rainfall regimes. *Quart. J. Roy. Meteor. Soc.,* **81,** 198–210.

Liu, P. C., 1994: Wavelet spectrum analysis and ocean wind waves. *Wavelets in Geophysics,* E. Foufoula-Georgiou and P. Kumar, Eds., Academic Press, 151–166.

Lorenz, E. N., 1991: Chaos, spontaneous climatic variations and detection of the greenhouse effect. *Greenhouse Gas-Induced Climatic Change: A Critical Appraisal of Simulations and Observations,* M. E. Schlesinger, Ed., Elsevier, 457–469.

Mak, M., 1995: Orthogonal wavelet analysis: Interannual variability in the sea surface temperature. *Bull. Amer. Meteor. Soc.,* **76,** 2179–2186.

Meehl, G. A., 1987: The annual cycle and interannual variability in the tropical Pacific and Indian Ocean regions. *Mon. Wea. Rev.,* **115,** 27–50.

——, 1997: The South Asian monsoon and the tropospheric biennial oscillation. *J. Climate,* **10,** 1921–1943.

Mooley, D. A., and B. Parthasarathy, 1984: Fluctuations in all-India summer monsoon rainfall during 1871–1978. *Climate Change,* **6,** 287–301.

Normand, C., 1953: Monsoon seasonal forecasting. *Quart. J. Roy. Meteor. Soc.,* **79,** 463–473.

Parker, D. E., M. Jackson, and E. B. Horton, 1995: The GISST2.2 sea surface temperature and sea-ice climatology. Hadley Centre for Climate Prediction and Research Tech. Rep. CRTN 63, 35 pp. [Available from Hadley Centre for Climate Prediction and Research, U.K. Meteorological Office, London Road, Bracknell, Berkshire RG12 2SY, United Kingdom.]

Parthasarathy, B., K. Rupa Kumar, and A. A. Munot, 1991: Evidence of secular variations in Indian monsoon rainfall–circulation relationships. *J. Climate,* **4,** 927–938.

Rasmusson, E. M., and T. H. Carpenter, 1982: Variations in tropical sea surface temperature and surface wind fields associated with the Southern Oscillation/El Niño. *Mon. Wea. Rev.,* **110,** 354–384.

Rayner, N. A., E. B. Horton, D. E. Parker, C. K. Folland, and R. B. Hackett, 1996: Version 2.2 of the Global Sea-Ice and Sea Surface Temperature Data Set, 1903–1994. Hadley Centre for Climate Prediction and Research Tech. Rep. CRTN 74, 35 pp. [Available from Hadley Centre for Climate Prediction and Research, U.K. Meteorological Office, London Road, Bracknell, Berkshire RG12 2SY, United Kingdom.]

Reynolds, R. W., and T. M. Smith, 1994: Improved global sea surface temperature analyses using optimum interpolation. *J. Climate,* **7,** 929–948.

Ropelewski, C. F., and P. D. Jones, 1987: An extension of the Tahiti–Darwin Southern Oscillation index. *Mon. Wea. Rev.,* **115,** 2161–2165.

Shukla, J., 1995: Predictability of the tropical atmosphere, the tropical oceans and TOGA. *Proc. Int. Sci. Conf. on the Tropical Ocean Global Atmosphere (TOGA) Programme,* WCRP-91, WMO/TD 717, Vol. 2, Melbourne, Australia, WCRP, 725–730.

——, and D. A. Paolino, 1983: The Southern Oscillation and long-range forecasting of the summer monsoon rainfall over India. *Mon. Wea. Rev.,* **111,** 1830–1837.

Simmonds, I., and P. Hope, 1997: Persistence characteristics of Australian rainfall anomalies. *Int. J. Climatol.,* **17,** 597–613.

Soman, M. K., and J. Slingo, 1997: Sensitivity of the Asian summer monsoon to aspects of sea surface temperature anomalies in the tropical Pacific Ocean. *Quart. J. Roy. Meteor. Soc.,* **123,** 309–336.

Torrence, C., and G. P. Compo, 1998: A practical guide to wavelet analysis. *Bull. Amer. Meteor. Soc.,* **79,** 61–78.

——, and P. J. Webster, 1998: The annual cycle of persistence in the El Niño–Southern Oscillation. *Quart. J. Roy. Meteor. Soc.,* **124,** 1985–2004.

Trenberth, K. E., 1976: Spatial and temporal variations of the Southern Oscillation. *Quart. J. Roy. Meteor. Soc.,* **102,** 639–653.

——, 1984: Signal versus noise in the Southern Oscillation. *Mon. Wea. Rev.,* **112,** 326–332.

——, 1997: The definition of El Niño. *Bull. Amer. Meteor. Soc.,* **78,** 2771–2777.

——, and D. J. Shea, 1987: On the evolution of the Southern Oscillation. *Mon. Wea. Rev.,* **115,** 3078–3096.

——, and J. W. Hurrell, 1994: Decadal atmosphere–ocean variations in the Pacific. *Climate Dyn.,* **9,** 303–319.

Troup, A. J., 1965: The ''southern oscillation.'' *Quart. J. Roy. Meteor. Soc.,* **91,** 490–506.

Wainer, I., and P. J., Webster, 1996: Monsoon/El Niño–Southern Oscillation relationships in a simple coupled ocean–atmosphere model. *J. Geophys. Res.,* **101,** 25 599–25 614.

Walker, G. T., and E. W. Bliss, 1937: World weather VI. *Mem. Roy. Meteor. Soc.,* **4,** 119–139.

Wang, B., 1995: Interdecadal changes in El Niño onset in the last four decades. *J. Climate,* **8,** 267–285.

——, and Y. Wang, 1996: Temporal structure of the Southern Oscillation as revealed by wave-form and wavelet analysis. *J. Climate,* **9,** 1586–1598.

Wang, X. L., and C. F. Ropelewski, 1995: An assessment of ENSO-scale secular variability. *J. Climate,* **8,** 1584–1599.

Webster, P. J., 1995: The annual cycle and the predictability of the tropical coupled ocean–atmosphere system. *Meteor. Atmos. Phys.,* **56,** 33–55.

——, and T. N. Palmer, 1997: The past and future of El Niño. *Nature,* **390,** 562–564

——, V. Magaña, T. N. Palmer, J. Shukla, R. A. Tomas, M. Yanai, and T. Yasunari, 1998: Monsoons: Processes, predictability and the prospects for prediction. *J. Geophys. Res.,* **103,** 14 451–14 510.

Wright, P. B. 1989: Homogenized long-period Southern Oscillation indices. *Int. J. Climatol.,* **9,** 33–54.

Yasunari, T., 1990: Impact of Indian monsoon on the coupled atmosphere/ocean system in the tropical Pacific. *Meteor. Atmos. Phys.,* **44,** 29–41.

——, and Y. Seki, 1992: Role of the Asian monsoon on the interannual variability of the global climate system. *J. Meteor. Soc. Japan,* **70,** 177–189.

Zebiak, S. E., and M. A. Cane, 1991: Natural climate variability in a coupled model. *Greenhouse Gas-Induced Climatic Change: A Critical Appraisal of Simulations and Observations,* M. E. Schlesinger, Ed., Elsevier, 457–469.

Zhang, Y., J. M. Wallace, and D. S. Battisti, 1997: ENSO-like interdecadal variability: 1900–93. *J. Climate,* **10,** 1004–1020.